LIGO Laboratory / LIGO Scientific Collaboration

LIGO-T1300688 Advanced LIGO 8/20/2013

ALS Noise Measurements and Model for HIFO-Y

Alexa Staley, Kiwamu Izumi, Stefan Ballmer

Distribution of this document:
LIGO Scientific Collaboration

This is an internal working note
of the LIGO Laboratory.

California Institute of Technology
LIGO Project – MS 18-34
1200 E. California Blvd.
Pasadena, CA 91125
Phone (626) 395-2129
Fax (626) 304-9834
E-mail: info@ligo.caltech.edu

Massachusetts Institute of Technology
LIGO Project – NW22-295
185 Albany St
Cambridge, MA 02139
Phone (617) 253-4824
Fax (617) 253-7014
E-mail: info@ligo.mit.edu

LIGO Hanford Observatory
P.O. Box 159
Richland WA 99352
Phone 509-372-8106
Fax 509-372-8137

LIGO Livingston Observatory
P.O. Box 940
Livingston, LA 70754
Phone 225-686-3100
Fax 225-686-7189

http://www.ligo.caltech.edu/

Contents

List of Tables

List of Figures

Acknowledgements: I would like to thank Kiwamu Izumi and Stefan Ballmer for help in creating the model, collecting some of the data, and editing the document. I would also like to extend an appreciation to Christopher Wipf, Matthew Evans, and Lisa Barsotti for guidance during the initial stages of the model. Lastly, I would like to thank Sheila Dwyer and Daniel Sigg for input on the documentation.

Abstract

Our measurements show a residual RMS of approximately 5 Hz for End-Y Half Interferometer (HIFO-Y). This matches well with the ALS model prediction. The dominant noise sources come from acoustic coupling at frequencies of around 100 Hz and suspension motion at frequencies below 5 Hz. The model indicates that with a reduction in acoustic noise by a factor of 10, the UGF of the CARM feedback control can be increased to 1 kHz while keeping under the noise requirement of 8 Hz. The model also highlights other contributing noise projections.

Besides noise projections, the ALS model is a linear control model that provides one with the ability to run several transfer functions of the servo loops required for the Arm Length Stabilization (ALS) system in HIFO-Y. This document describes the model and noise analysis in detail. Section 1 provides general information about the model. In Section 2, the specific loops of the model are discussed. And finally in Section 3, the noise measurements are examined.

1 Overview of the Model

The purpose of the ALS model is to establish a noise budget for HIFO-Y. Specifics about ALS, arm locking, and HIFO-Y can be found in [1], [2], and [3] respectively. The model, which is a linear control model, replicates all the feedback servos utilized in HIFO-Y locking. In addition to being used for noise budgeting, the model provides several transfer functions of a variety of different servo loops.

The control model can be divided into several sections including:

1. End Y FIBR servo: uses a phase locked loop (PLL) to lock the auxiliary laser to the frequency transmitted fiber light with a frequency offset
2. End Y REFL servo: uses Pound-Drever-Hall (PDH) to lock the green laser light to the arm cavity
3. IMC REFL servo: locking the pre-stabilized laser (PSL) to the input mode cleaner (IMC) using the reference cavity AOM and the mode cleaner length.
4. MC2 Filters: suspension filters and actuators for MC2
5. Slow path REFL servo loop: controls the interferometer common mode for the common arm (CARM) feedback
6. Beat detector: locks the corner Voltage Controlled Oscillators (VCOs) to the green beat note controlling the common mode

Fig. 1 is an image of the simulink model. The different sections listed above are highlighted in various colors. Details about the model configuration can be found in Appendix A.

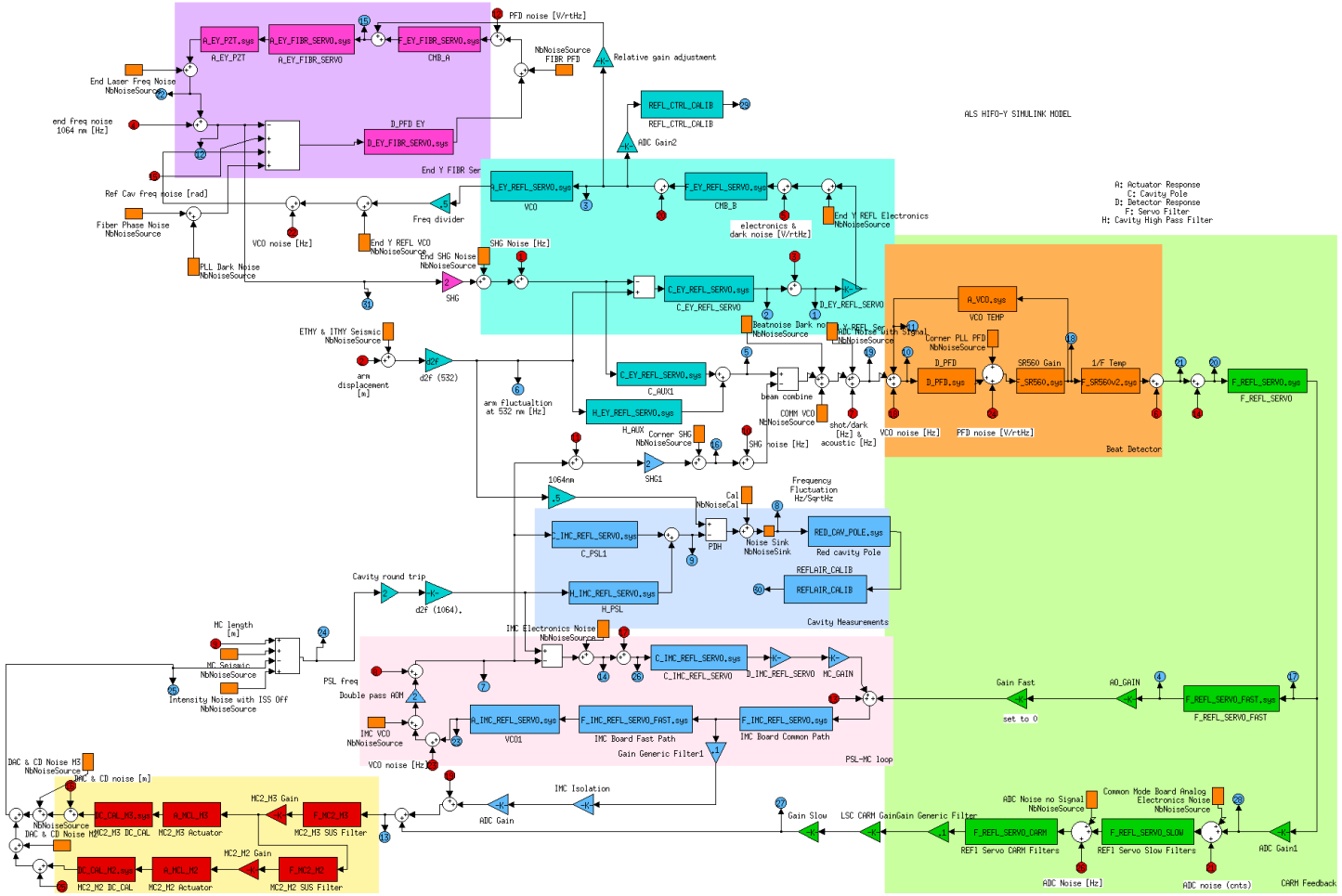

Figure 1: Image of ALS simulink model

Table 1: Notation

Abbreviation	Description
A	Actuator Response
C	Cavity Pole
D	Detector Response
F	Servo Filter
H	Cavity High Pass Filter

2 Control Loops

This section provides a detailed description of the highlighted portions in Fig. 1. First, the servo loops in the End Y station are discussed, followed by those in the corner station. Measured transfer functions of the individual loops are provided along with those produced by the model. In addition to these transfer functions, one can also find power spectrums of the locked loops. Finally, this section concludes by examining the global control of the model.

The measured transfer functions described in this section were taken with SR785s in the swept sine configuration. The source amplitude ranged from about 50mV to 100mV depending on the saturation of the signal and stability of the loop. The excitation was injected into excitation A of all the boards and the transfer functions were read using test points 1 and 2. All the transfer functions of the loops were taken when the respective feedback was locked. For example, the transfer function of the End Y REFL servo was taken when both the End Y PLL and PDH loops were locked, while the transfer function of the End Y Fiber servo was taken while only the End Y PLL loop was locked (see Section 2.1). Similarly for the loops in the corner station (see Section 2.2). All the boards were in the settings indicated in Table 3. For validating the global control of the model, as described in Section 2.3, the measurement was taken by exciting H1:LSC-Y_EXTRA_AO_1, which was connected to the excitation A input of the End Y REFL common mode board, and reading out H1:LSC-REFLAIR_A_RF_9_I_OUT with a reference of H1:ALS-Y_REFL_CTRL_OUT_DQ. This measurement was taken with the cavity arm locked to the green beam after handing off to the CARM control with the infrared beam resonant in the cavity.

2.1 End Y

The End Y servos consist of the FIBR and REFL servos, which will be examined separately in this section. There exists an additive offset (AO) between the two loops, which will be motivated in Section 2.1.2. The signal from the fast path of the REFL common mode board (CMB) is sent to the Voltage Controlled Oscillator (VCO); meanwhile, a signal picked off at the test point right before the fast path of RELF CMB is sent to the excitation A input

of the FIBR CMB.

2.1.1 End Y FIBR Servo Loop

The End Y FIBR servo employs a phase locking loop (PLL) scheme. The PLL locks the 1064 nm light of the end station auxiliary laser to the PSL frequency, which is transmitted to the end station via a single-mode optical fiber. The FIBR servo loop in the model is designated in the purple section of Fig. 1. The servo filter, which is tuned for locking, has a frequency response of $F_{EY\_FIBR\_SERVO}$. Meanwhile, the piezo-electric actuator has a response of A_{EY_PZT}. And finally, the PLL detector response is dictated by the phase frequency discriminator and is given by $D_{EY\_FIBR\_SERVO}$.

Fig. 2 is a graph of the measured End Y FIBR servo open-loop gain transfer function and that produced by the model. The dark blue line shows data collected with an audio frequency spectrum analyzer, while the light blue and red lines show data collected with an RF spectrum analyzer. The red line is measured with the generic filter of the FIBR common mode board turned on. Clearly, this low pass filter is important in preventing additional unstable UGFs from appearing. It is evident that the UGF is approximately 18 kHz with a phase margin of above 45 degrees. The magnitude and phase of the measured transfer function are almost equivalent to the model until around 100 kHz. Above 100 kHz, the data exhibits a PZT resonance structure as seen by the reproducible fluctuations in the plot.

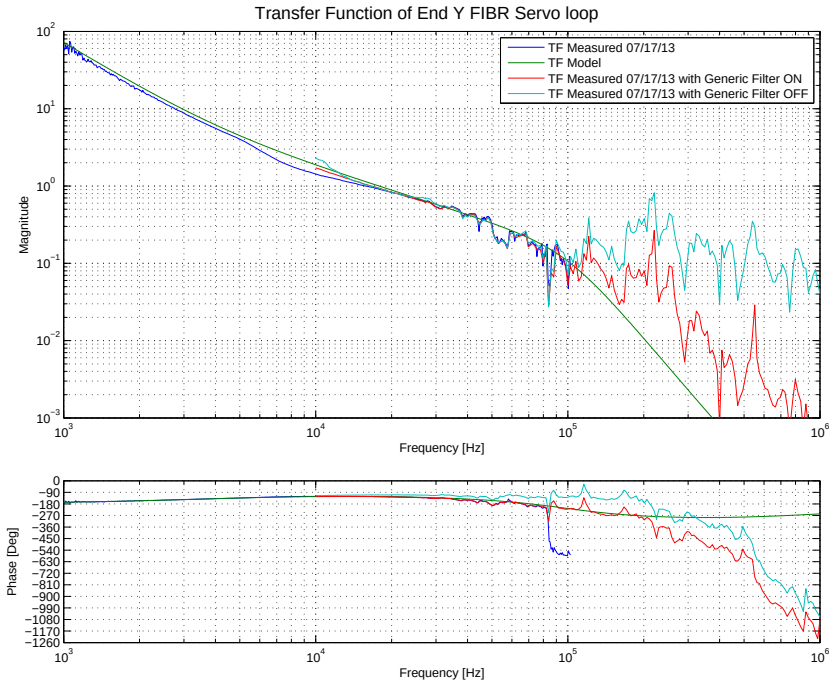

Figure 2: Open Loop Transfer Function of End Y FIBR Servo

Fig. 3 and Fig. 4 are graphs of the power spectrum measured at the error point of the End Y FIBR servo loop measured on July 17, 2013 and July 25, 2013 respectively. The two plots should be the same; it is unknown what changed the behavior. The only difference between the two measurements was the channel input used on the SR785.

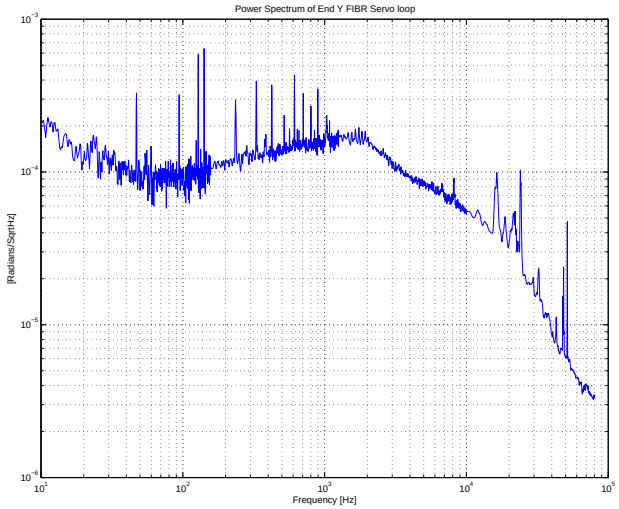

Figure 3: Power Spectrum of End Y FIBR Servo Loop (07/17/13)

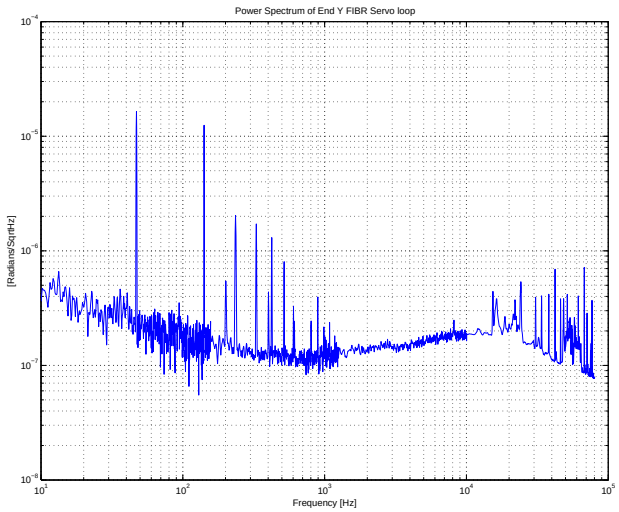

Figure 4: Power Spectrum of End Y FIBR Servo Loop (07/25/13)

Note, more on this servo loop can be read in [4].

2.1.2 End Y REFL Servo Loop

The End Y REFL servo employs a Pound-Drever-Hall (PDH) locking scheme (see [5] for details on PDH) to lock the 532 nm light of the auxiliary laser to the arm cavity. This loop is highlighted in cyan in Fig. 1. Again, the servo filter, which is tuned for locking, has a frequency response of $F_{EY\_REFL\_SERVO}$. Meanwhile, the laser frequency actuator has a response of $A_{EY\_REFL\_SERVO}$. From [6], the cavity frequency response can be approximated as a single-pole low pass filter,

$$C_{EY\_REFL\_SERVO} = \frac{1}{1 + i(f/f_c)} \tag{1}$$

where f is the frequency of the signal and f_c is the cavity pole frequency, which was measured to be 600 Hz in this case. Finally, the detector response is given by $D_{EY\_REFL\_SERVO}$.

Fig. 5 is a graph of the End Y REFL servo open loop transfer function measured with an SR785 and that produced by the model with both the AO on and off. It evident that the UGF is 12 kHz. Given the improved phase margin with the AO on, this is the preferable set-up. In addition, from this graph we see a generally nice agreement between the model and the data collected except for the flatness that appears near the UGF with the AO on. This flatness is due to a slightly lower End Y FIBR servo UGF than in the model, or gain peaking (see Fig. 2).

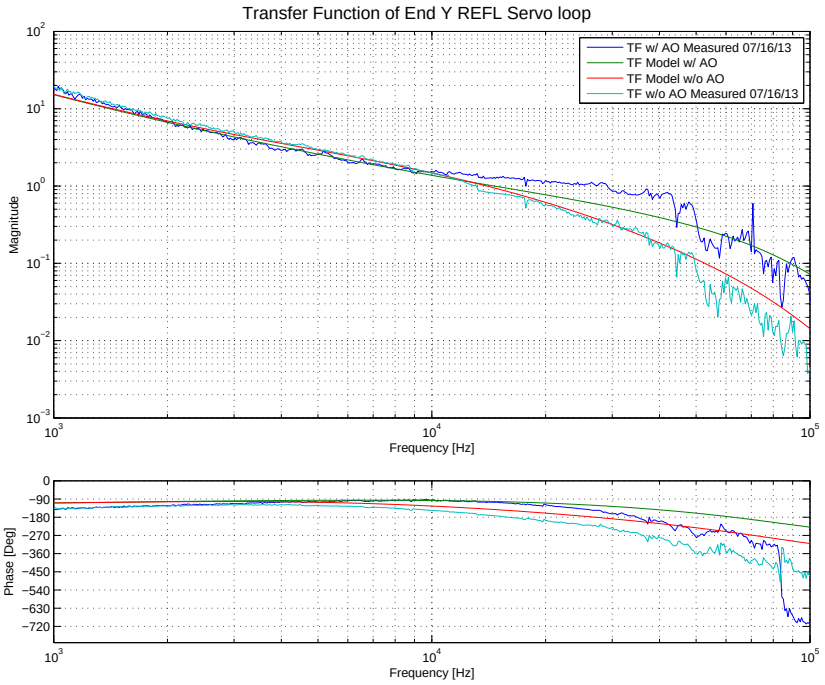

Figure 5: Open Loop Transfer Function of End Y REFL Servo Loop with the Additive Offset both Off and On.

Fig. 6 is a graph of the power spectrum measured at the error point of the End Y REFL servo loop with the AO off and on. We see gain peaking with both the AO on and off, but more so with the AO off as expected from the closed loop transfer functions depicted in Fig. 7. There appears to be some resonance structure near 20 kHz as well with the AO on.

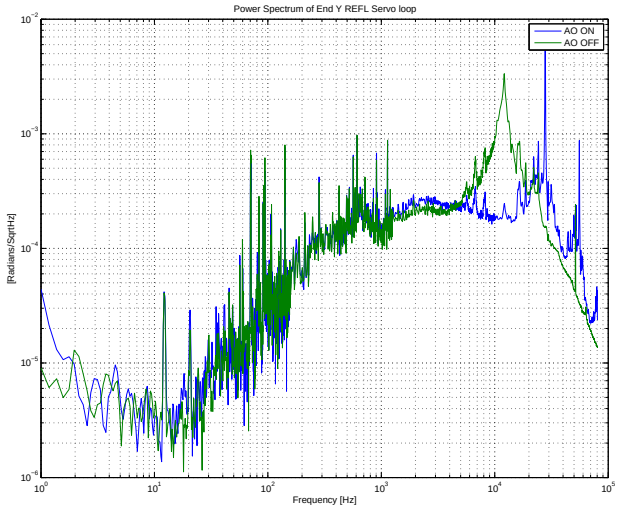

Figure 6: Power Spectrum of End Y REFL Servo Loop with AO off and on (07/17/13)

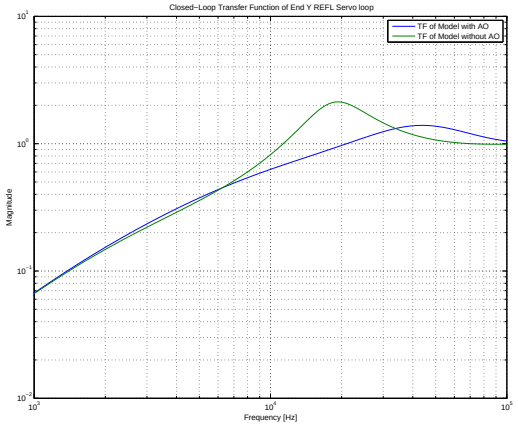

Figure 7: Closed Loop Transfer Function of End Y REFL Servo Loop with the additive offset both off and on.

Upon collecting the data in Fig. 6, we decreased the gain of the common mode board to -4 dB to -8 dB. With this new configuration, additional data was collected on July 25,

2013. Fig. 8 is the subsequent power spectrum. Again, one can see the decrease in noise with the AO on versus with the AO off. The noise around the UGF of the loop does not seem to decrease between the two gain settings, as depicted by the green and blue lines. As seen between the two sets of collected data for the End Y FIBR servo loop (Fig. 3 and Fig. 4), there is an overall factor of around 10^2 difference in noise between Fig. 6 and Fig. 8 as well. As mentioned in Section 2.1.1, the only difference between the two measurements was the channel input used on the SR785.

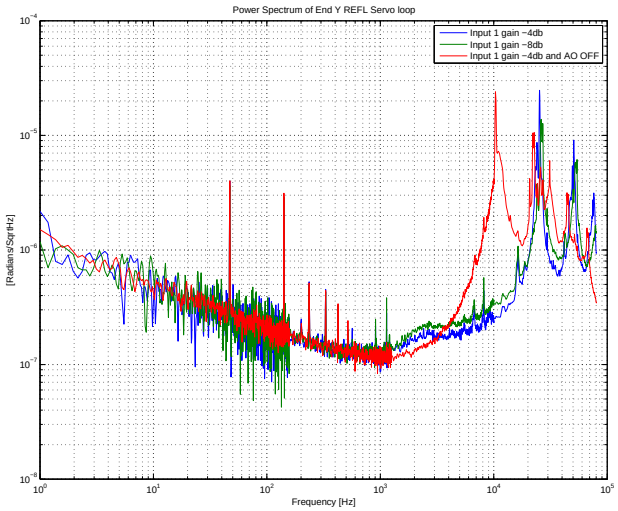

Figure 8: Power Spectrum of End Y REFL Servo Loop (07/25/13)

2.2 Corner

The corner station servos consist of the CARM feedback path, the beat detector, the PSL-MC loop, and the MC2 filters. The loops are highlighted in green, orange, blue/yellow, and red respectively in the model.

2.2.1 REFL Servo Loop

The REFL servo loop consist of both fast and slow servo filters given by $F_{REFL\_SERVO\_FAST}$ and $F_{REFL\_SERVO\_SLOW}$ respectively, along with the common servo filter given by F_{REFL_SERVO}. Currently, the fast path is deactivated, and only the slow path is used in the CARM feedback. The CARM feedback controls the common length of the arm cavity. This control signal is produced by performing a heterodyne measurement between the 532 nm light and a frequency-doubled sample of the PSL light.

Additionally, this loop contains a PLL-based frequency sensor as highlighted in orange of Fig. 1 and drawn in Fig. 9. The poles and zeros in this image are not up to date (see Table 3 for the correct zero/pole pairs). This loop was designed with two SR560s and a low noise VCO unit. Ultimately, the SR560s will be replaced with a board. The UGF of this loop was measured to be 60 kHz. As usual, the detector response is given by D_{PFD} for the phase frequency discriminator. Meanwhile, the actuator response and servo filter response are given by A_{VCO} and F_{SR560} respectively.

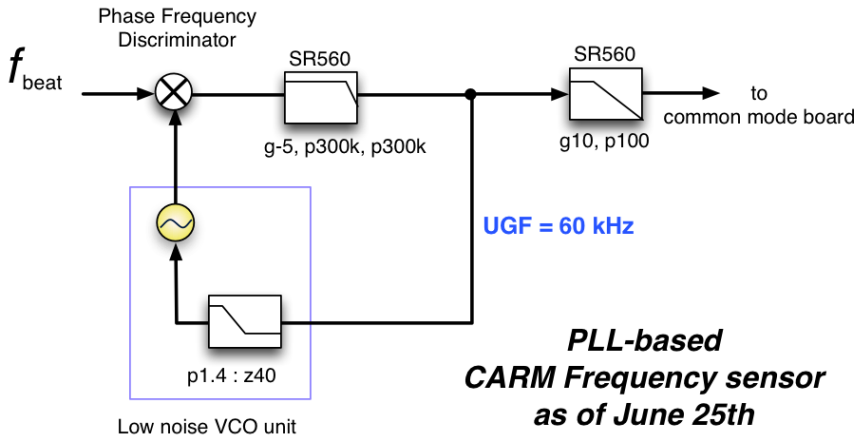

Figure 9: Image of PLL-based CARM Frequency Loop (alog 6882)

Fig. 10 is an open loop transfer function of the corner PLL measured with an SR785 and that produced by the model. This data was measured and compared to the model using 45 deg/V for the phase frequency discriminator coefficient ([7]) and following the zero/pole pairs as depicted in Fig. 9 (different from Table 3). The data and model are equivalent; however, the phase differs at high frequency. This discrepancy is due to a time delay not included in the model.

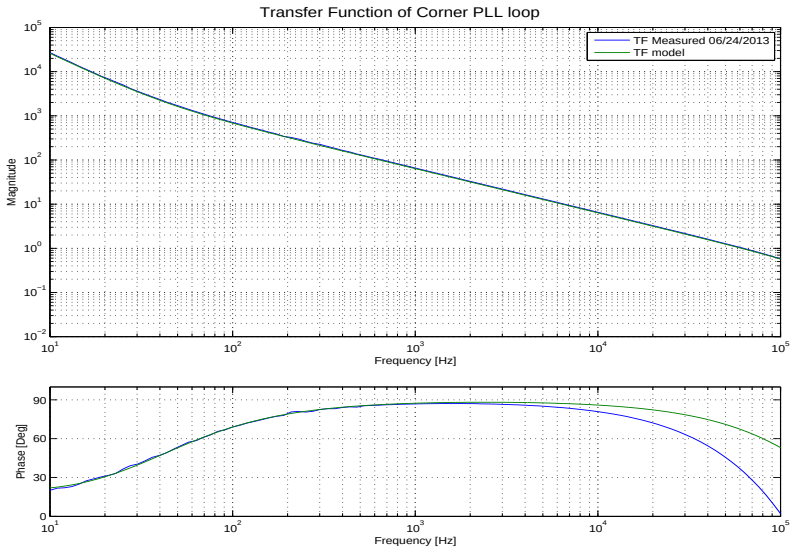

Figure 10: Open Loop Transfer Function of PLL Corner Loop

Fig. 11 is a graph of the open loop transfer function of the Slow REFL Servo loop with the CARM feedback in place. The green line shows data measured via the front end system; meanwhile, the blue line is that produced by the model. The model matches the overall structure of the data; however, it appears to have a steeper slope after the kink at 20 Hz. There is also a mystery gain of 8.46 present in LSCCARM, used in order to replicate the UGF of the data. The discrepancy between the measurement and the model could be due to saturation of the data. The UGF of the loop is just below 200 Hz with a phase margin of about 30 degrees.

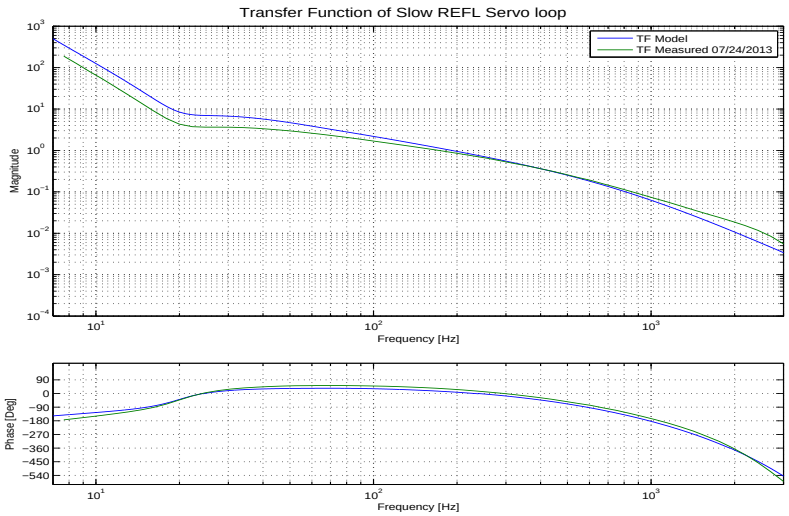

Figure 11: Open Loop Transfer Function of Slow REFL Servo Loop

2.2.2 IMC REFL Loop

The input mode cleaner (IMC) REFL loop locks the pre-stabliized laser (PSL) to the mode cleaner length. This path is not used for the CARM control; but is necessary for the original locking of the PSL. Again, $F_{IMC\_REFL\_SERVO}$ is the response of the common path servo filter. Meanwhile, $F_{IMC\_REFL\_SERVO\_FAST}$ is the response of the fast path servo filter. As with the arm cavity, the MC cavity can be approximated by a single-pole cavity response given by $C_{IMC\_REFL\_SERVO}$. In this case, the cavity pole is at 8812.36 Hz (alog 5429). Lastly, the actuator response is given by $A_{IMC\_REFL\_SERVO}$.

Fig. 12 is a graph of the transfer function of the IMC open loop gain. The green line is the transfer function measured by an SR785, while the blue is that produced by the model. Again the data and model produce similar results. (Note: if the zero of the second boost stage in the model is changed from 20 kHz to 10 kHz the model matches the data significantly better). The UGF of this loop is about 25 kHz.

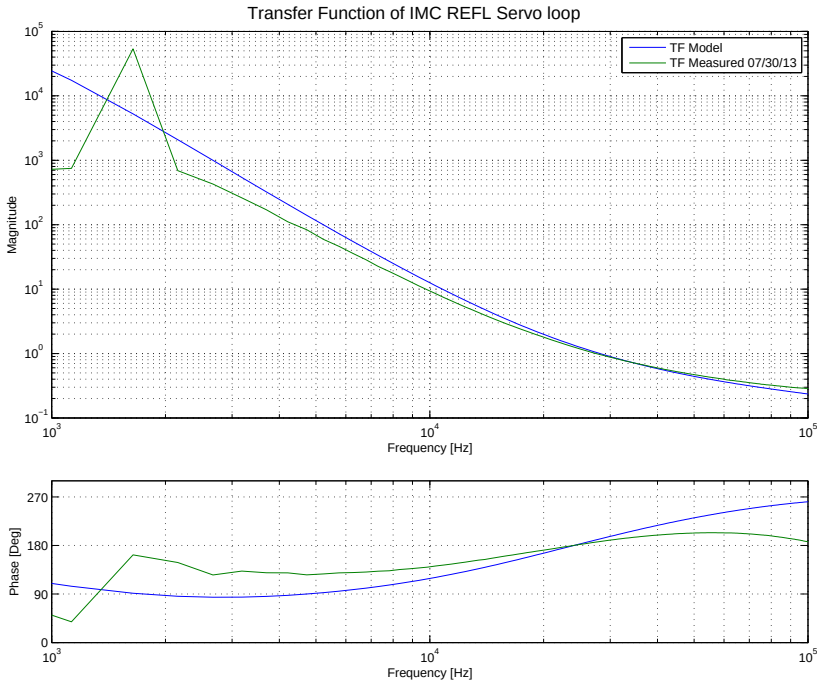

Figure 12: Open Loop Transfer Function of IMC Loop

2.2.3 MC2 Filters and Actuators

The MC2 suspension loop is highlighted in yellow in Fig. 1. This loop contains the filter and actuators for the second and third stage suspensions of the second test mass in the mode cleaner. The transfer functions for the MC2 suspensions can be found in [8].

2.3 Validating Global Control

Fig. 13 is a transfer function from the end station frequency noise to the reflected infrared beam. The transfer function was taken by exciting excitation A input on the End Y REFL Servo board and reading out through H1:LSC-REFLAIR_A_RF_9_I_OUT (calibrated in Hz) with a reference of H1:ALS-Y_REFL_CTRL_OUT_DQ. The arm cavity length can be derived from (alog: 7187),

$$\text{Cavity Length} = \lambda \left(\frac{L}{c} \right) \times \text{H1:ALS-Y\_REFL\_CTRL\_OUT\_DQ} \tag{2}$$

where $\lambda = 532$ nm for green light, $L = 4$ km and c is the speed of light. Meanwhile, H1:LSC-REFLAIR_A_RF_9_I_OUT reads out the I phase from the in air resonant PD of the reflected infrared light [9].

Fig. 13 is graph of the afore-mentioned transfer function and that produced by the model. Both lines exhibit a $1/f^3$ behavior at around 500 Hz. From 200 Hz to around 1 kHz, the phase of the two match sufficiently. The magnitude of the model is more believable than the measured data. At low frequency we see a flat unity response from the end station loops below the UGF, and then we see a suppression from the arm cavity pole, and finally the influence of the CARM feedback at high frequency.

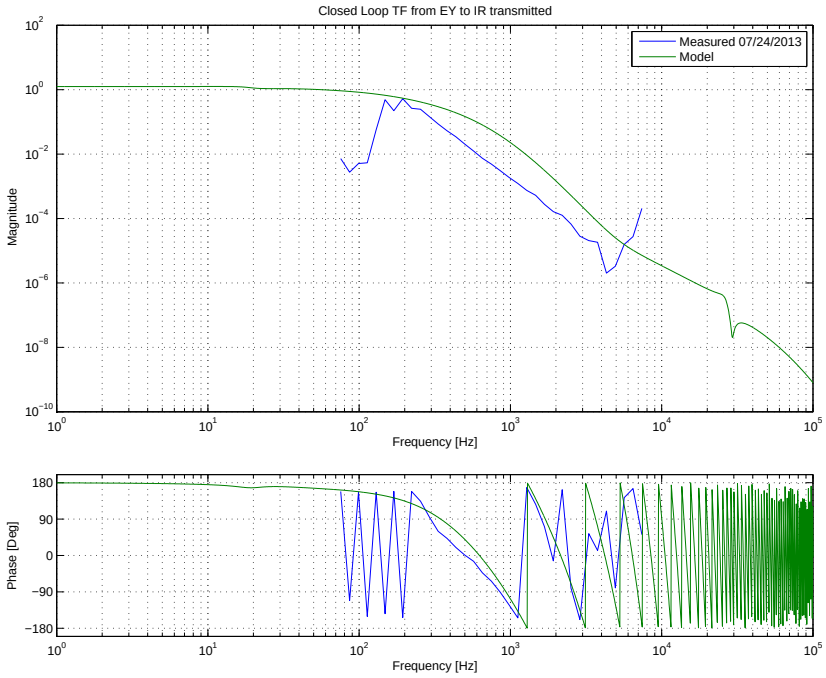

Figure 13: Closed Transfer Function from End Y to Infrared Reflected

Note, the measurement is only coherent from around 300 Hz onwards.

3 Noise Budget

This section describes the noise sources that may limit the performance of the control system. Noise measurements were taken for the following potential sources:

1. Residual laser noise of the End Y REFL servo loop
2. Fiber noise (see [10])
3. End Y FIBR dark noise
4. End Y FIBR PFD noise
5. Corner PLL PFD noise
6. End Y REFL demodulator electronics and dark noise – measured while blocking the beam at the diode
7. COMM VCO, End Y REFL VCO, and IMC VCO (see [11])
8. Corner and End SHG noise
9. ADC Noise
10. DAC and Coil Driver noise of MC2 M3 and M2
11. Beat note dark and electronic noise
12. Measured out of loop IR noise
13. IMC transmitted frequency noise with closed loop correction
14. IMC dark and electronic noise
15. IMC, ETMY, ITMY seismic

Fig. 14 consists of several noise measurements in the ALS model above 10^{-4} Hz/$\sqrt{\text{Hz}}$; the remaining noise sources are well below the noise requirement of 8 Hz and are not major contributors. The noise measurements are all calibrated and plotted in Hz/$\sqrt{\text{Hz}}$ for the infrared beam.

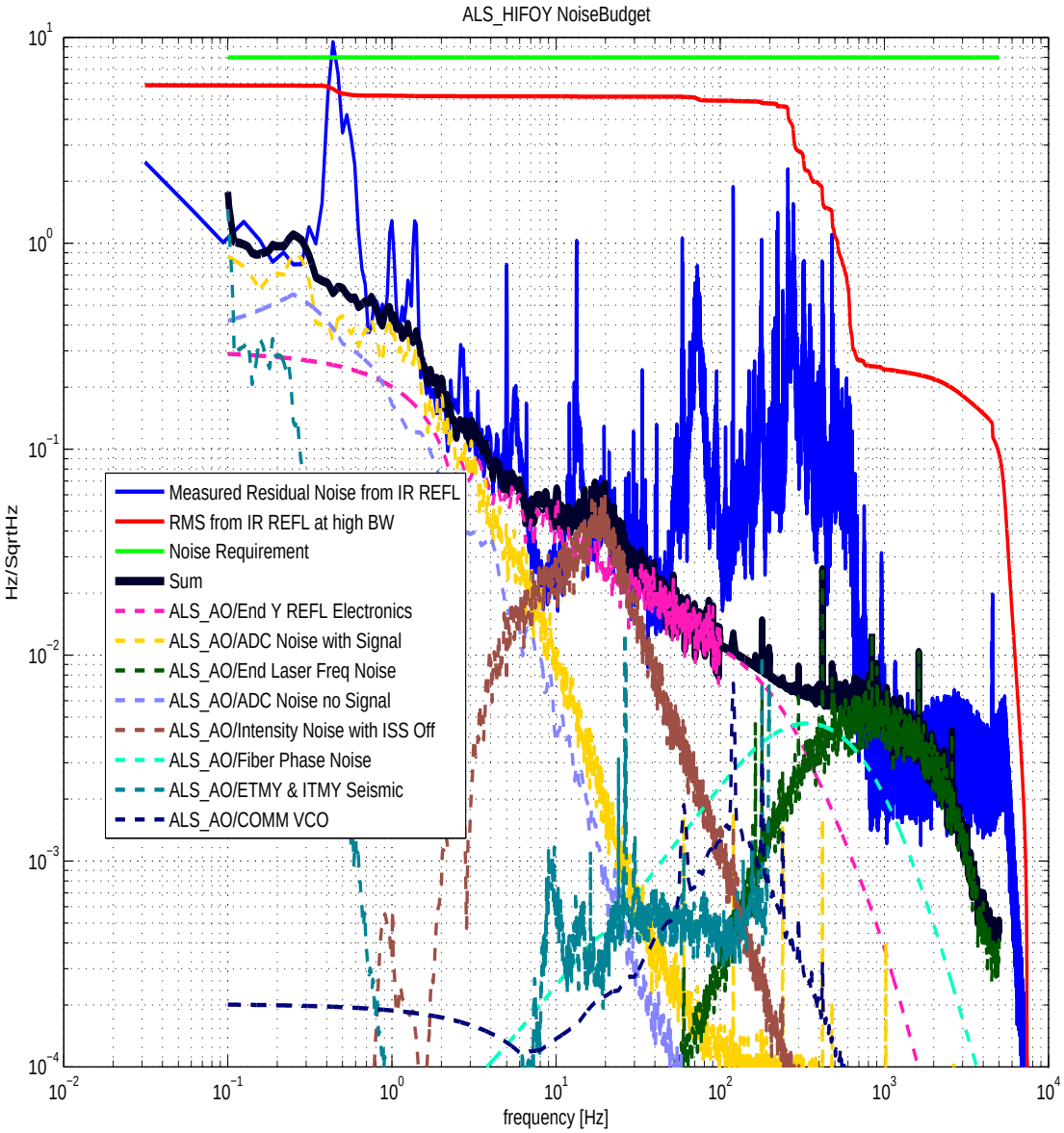

Figure 14: Noise Spectrum

3.1 Measurements

The noise measurements listed above are taken by multiplying the amplitude spectral density of the source with the transfer function originating at the noise source and terminating at the out-of-loop measured residual fluctuation (output 8 on Fig. 1) [6]:

$$n(f) = X(f)\sqrt{S(f)}. \tag{3}$$

In this equation, $S(f)$ is the power spectrum of a noise source and $X(f)$ is the transfer function described in equation (11). The noise sources were measured in a variety of different ways depending on the source.

3.1.1 Residual Laser Noise

The majority of the PSL and auxiliary laser frequency noise is suppressed by the control loops. However, due to the coupling between the control loops, some laser frequency noise from the auxiliary laser will contribute to the overall noise budget [6]. The "End laser frequency" noise indicates the frequency noise of the auxiliary laser in the End Y REFL servo loop. This noise is measured while the loop is locked, and then we assume that this noise consists of the unsuppressed laser fluctuations.

The data for this noise projection was imported from the channel H1:ALS-Y_FIBR_CTRL_OUT. In the model, this source was injected into input 4 through to output 8.

3.1.2 Fiber Noise

The fiber noise source was assumed to be 1 Hz/$\sqrt{\text{Hz}}$ following [10]. This source was injected into input 15 through to output 8.

3.1.3 Photodiode Dark noise

The End-Y FIBR servo loop PD dark noise was measured by examining the amplitude of the beat signal and determining the noise floor of the phase-frequency discriminator (PFD). The floor was found to be -73 dBm with 300 kHz band-width. This noise was converted to 91nVrms/$\sqrt{\text{Hz}}$. Meanwhile the amplitude of the beat signal was measured at 40 MHz. The signal found was -18 dBm and converted to 40 mV_p. The power spectrum was then computed via

$$S(f) = \frac{2S_v(f)}{V_{RF}^2} f^2 \tag{4}$$

as taken from equation 6.13 of [6]. In the above equation, S_v is the input-referred voltage noise and V_{RF} is the voltage amplitude of the main RF signal. Applying the aforementioned beat signal amplitude and dark noise floor to equation (4) gives the amplitude spectral density, $\sqrt{S(f)}$, used in equation (3). In the model, the source was injected into input 15 through to output 8.

This same technique was applied to the beat note PD dark noise. The RF power of the signal was measured to be -24 dBm which was converted to 12 mVp. Meanwhile, the noise floor out of the BBPD was -139 dBm/Hz at 80 MHz, which was converted to 25 nVrms/$\sqrt{\text{Hz}}$. In the model, this source was injected into input 7 through to output 8.

3.1.4 Phase-Frequency Discriminator Noise

The END Y FIBR and corner PFD noise were measured from the actual PFD board. For the end station, this source was injected into input 12 through to output 8. Meanwhile, in the corner station, this noise source was injected into input 24 through to output 8.

3.1.5 End Y REFL electronics

The PDH demodulator electronics and dark noise was measured while blocked the beam at the diode. This noise source was injected at input 5 of the model through to output 8.

3.1.6 Voltage Controlled Oscillator

The noise produced by the several voltage controlled oscillators in the control system was determined by importing data collected from [11]. The phase noise that was previously measured was given in dBc. The following conversion into amplitude spectral density was then performed:

$$\sqrt{S(\theta)} = 10^{\frac{dBc}{20}} \tag{5}$$

$$\sqrt{S(f)} = \sqrt{S(\theta)}\sqrt{2}f \tag{6}$$

where $\sqrt{S(\theta)}$ is given in rad/$\sqrt{\text{Hz}}$ and $\sqrt{S(f)}$ is given in Hz/$\sqrt{\text{Hz}}$. In the model, these sources were injected into input 7, 22, and 23 through to output 8 for the corner station, end station, and IMC VCOs respectively.

3.1.7 Second Harmonic Generation Noise

Both the end station and corner stations have second harmonic generators (SHG) used to double the frequency of the 1064 nm laser. It is assumed that both SHG's add to the laser frequency noise of this frequency doubled beam. [12] indicates an upper limit of the noise level to be $1 \times 10^{-5} f\text{Hz}/\sqrt{\text{Hz}}$. The SHG noise is present both in the end and corner station. In the end station, frequency doubling happens at the output of the auxiliary laser. Meanwhile, at the corner station, the PSL frequency is doubled for beat-note detection. The end station SHG noise is significantly less than the corner SHG noise since the former is suppressed in the End Y REFL Servo loop. Thus, only "Corner SHG" is plotted in Fig. 14. For the end station SHG, this source was injected into input 1 through to output 8. Meanwhile for the corner station, this source was injected into input 10.

3.1.8 ADC Noise

Several ADC noise measurements were taken. The "ADC Noise no Signal" is the ADC noise of the REFL_SERVO_SLOW channel with the DB9 cable disconnected. Meanwhile, the "ADC noise with signal" is the combined noise of the ADC, the CM board, and the signal generator. Whereas "Common Mode Board Analog Electronics" is the CM board by itself. There is some signal dependent noise in the ADC or CM board. During all the measurements, both the arm cavity and IMC were unlocked. In the model, the sources were injected into input 7, 26, 21 through to output 8 for ADC noise with signal, with no signal, and CMB analog electronics noise respectively.

3.1.9 DAC and Coil Driver Noise

The DAC and Coil Driver noise source for MC2 M3 and M2 stages were modeled to fit the data of Fig. 15.

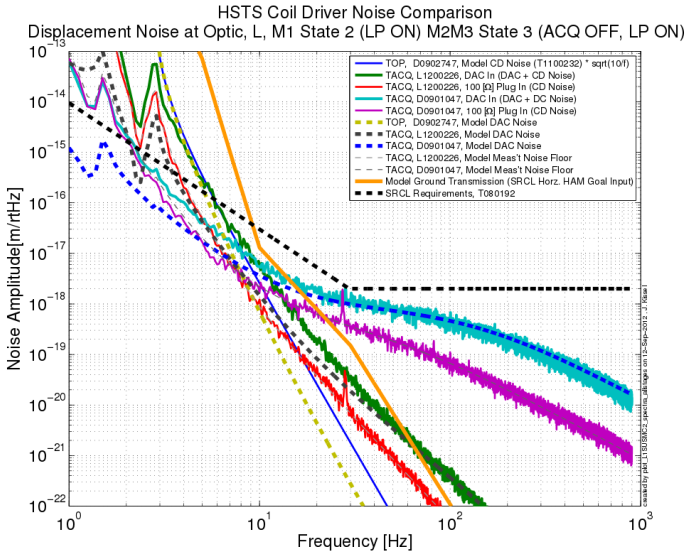

Figure 15: DAC and Coil Driver Noise for MC2

The noise amplitude was measured in meters and thus inserted into input 16 and 24 through to output 8 in the model for M3 and M2 stages respectively.

3.1.10 Measured out of loop IR Noise

This data was loaded from H1:LSC-REFLAIR_A_RF9_I_ERR under the configuration described in alog 7216. The alog indicates that this data (brown line in alog) was measured

under the infrared control configuration, meaning that the CARM is controlled via the infrared REFL demod signal and the ALS beat-note serves as an out of loop sensor. In order to compare this data to other noise projections in the model, this data is calibrated for the infrared beam.

3.1.11 IMC electronic noise

This noise was measured while the IMC common mode board input was turned off and the cavity was unlocked. The power spectrum from the fast output of the board was measured with an SR785. This data was injected into input 17 of the model through to output 8.

3.1.12 IMC Seismic

This data was imported from H1:IMC_X_DQ channel and then multiplied by the inverse whitening filter. In addition, this source was injected into input 9 through to output 8.

3.1.13 ETMY/ITMY Seismic

This data was imported from the seismic teams previous measurements:
/ligo/svncommon/SeiSVN/seismic/BSC-ISI/H1/ETMY/Data/Spectra/Isolated/
H1_ISI_ETMY_Y_Direction_Perf_For_ISC_Noise_Budget_20130806.mat.
This data was collected with the test masses in the isolated stages. This source was injected into input 2 through to output 8 in the model. It was assumed that the data would be similar for ETMY and ITMY.

3.1.14 Intensity Noise with ISS off

With the ISS off, the PSL intensity noise was measured as mentioned in alog 7364 (black line). This data was imported and calibrated into IMC length using the following prescription:

$$Data = Data \times \frac{L}{f_0} \tag{7}$$

where $L = 16.4736$ m for the IMC length (one way), and $f_0 = 2.818 \times 10^{14}$ Hz for the infrared frequency. The source was injected into input 9 through to output 8.

3.2 Estimated Acoustic Noise

In the overall measured residual noise (blue line in Fig. 14), there exists a large structure from around 50 Hz to 500 Hz that is assumed to be due to acoustic noise in the corner station. The acoustic noise source is expected to come from table motion and periscope resonance. One can infer the power spectrum of the acoustic noise source by taking this noise budget data and multiplying it by the inverse transfer function of input 7 to output 8 on Fig. 1. The result is given in Fig. 16.

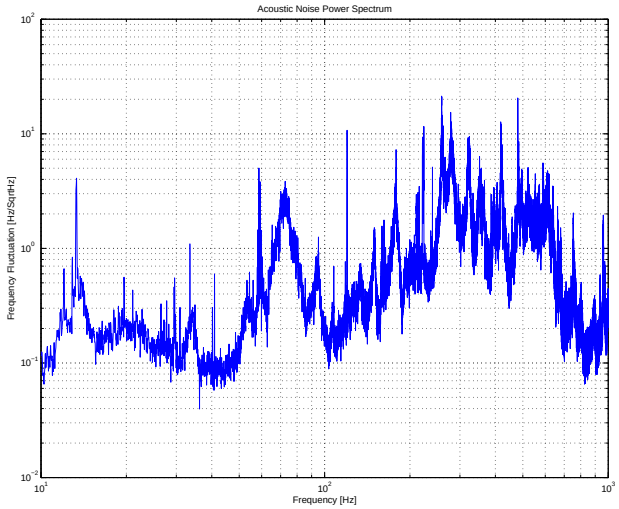

Figure 16: Estimated Acoustic Noise at the Green Beat-note, Calibrated for 532 nm

3.3 Analysis of Results

In Fig. 14, several of the measured noises are suppressed at high frequencies near the UGF of the REFL servo slow path, as desired. Recall in Section 2.2.1 that the REFL SERVO fast path was disabled in order to avoid injecting noises at high frequencies coming from the corner station.

Notably, the End Y REFL electronics noise appears to be relatively high given the overall out of loop measured residual noise. In particular, at around 10 Hz, the electronics noise is above this out of loop noise. The electronics noise was measured on July 3rd while blocking the beam at the diode and the transfer function was taken by injecting the noise at input 5 through to output 8 on Fig. 1. One possible suspect is the calibration of D_EY_REFL_SERVO. This detector response of the End Y Servo loop was never measured directly, but was calibrated in order for the open loop transfer function of the model to match that of the data. The electronic noise is injected into the model after this response, and is the most likely candidate for the suspiciously large noise budget.

Examining the measured residual noise from the IR reflected beam (blue line), we can attribute the noise peaks to several factors. The large structure in noise from 50 Hz to 500 Hz is due to acoustic coupling in the corner station. In particular at around 60Hz we have acoustic coupling from the periscope resonance, and around 300 Hz we have acoustic coupling from table motion and the mirrors (see Section 3.2). Meanwhile, at lower frequencies, several of the peaks are as a result of the mechanical motion in the quad

suspensions (see [8] for reference). In particular,

- 0.43 Hz due to longitudinal resonance
- 0.56 Hz due to pitch motion
- 5 Hz due to quad trans/roll that is undamped
- $\sim$ 5 Hz resonance of the building that is excited by wind (see slog 7150)

As a nice comparison, Fig. 17 is a plot of the sum of all the noise projections depicted in Fig. 14, along with the overall measured residual noise (blue line in Fig. 14). Note, that the sum of all the noises was computed as follows,

$$SumNoise = \sqrt{\sum_i (S_i^2)} \tag{8}$$

where i are the types of noises and S_i is the noise projection of a particular noise. The results are consistent with the exception that the measured residual noise includes the suspension noises and the acoustic noise as discussed above.

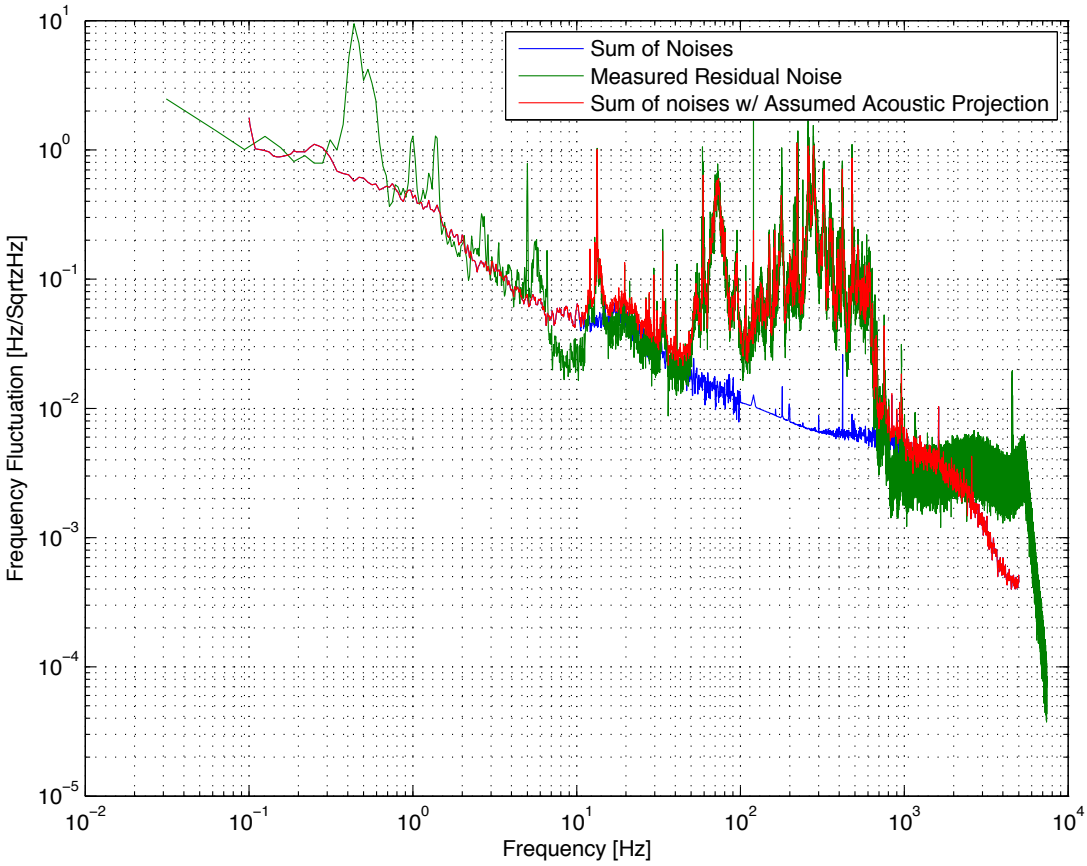

Figure 17: Sum of all Noise vs. Measured Residual Noise

3.4 CARM Feedback Loop

One limitation of the CARM feedback loop is sensor noise. This sensor noise is dominated by acoustic noise, ADC noise, end laser frequency noise, fiber noise, and end REFL electronics noise. Fig. 18 is a graph consisting of all these noise sources before applying the CARM control. As a result, one does not see the knee/suppression at high frequencies as seen in Fig. 14 for these same sources.

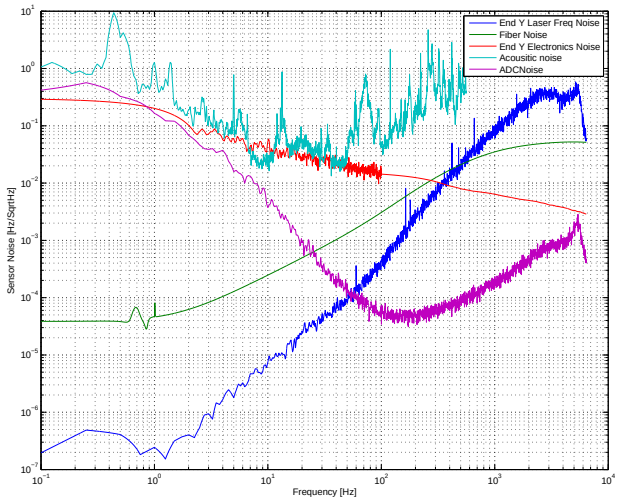

Figure 18: Sensor Noise Before Applying CARM Control.

From this sensor noise, one can compute the infrared noise of the CARM control. In particular,

$$S_{infrared\_noise}(f) = \frac{G}{1+G} \times S_{sensor\_noise}(f). \tag{9}$$

For simplicity, this can be approximated by,

$$S_{infrared\_noise}(f) = S_{sensor\_noise}(f) \times \begin{cases} 1, & \text{if } f < \text{UGF} \\ \text{UGF}/f, & \text{if } f > \text{UGF}. \end{cases} \tag{10}$$

This assumes a $1/f$ behavior above the UGF of the CARM feedback which overestimates the RMS. From Fig. 11 the UGF of the CARM feedback is 150 Hz. Using this UGF, Fig. 19 is a plot of the infrared noise as a function of frequency. Examining the blue and red lines, one can see the dominating features of the quad suspension noise at low frequencies and the End Y laser frequency noise (prior to applying the CARM control) at high frequencies. Again, from around 50 Hz to 500 Hz, acoustic coupling is the main noise contributor. The blue line includes the current acoustic noise from Fig. 16, meanwhile the red line is plotted with the acoustic noise in the regime of 10 Hz to 1 kHz reduced by a factor of 10 predicted for the science run.

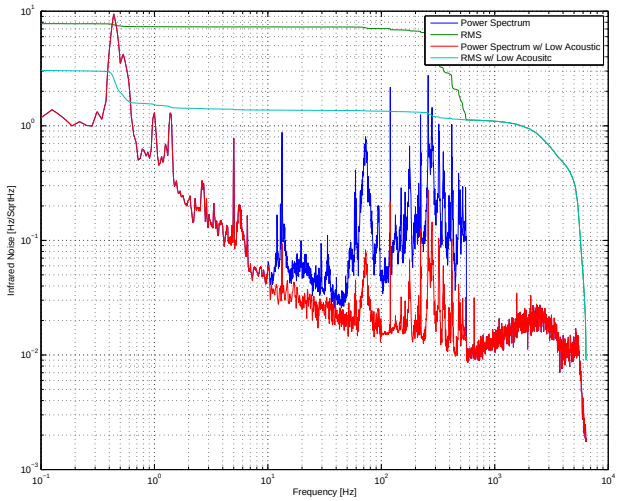

Figure 19: Infrared Noise Assuming 150 Hz UGF for CARM Feedback

In Fig. 19, the green and cyan lines are the RMS for the blue and red lines respectively. Notice, the green RMS line matches with the RMS line in Fig. 14 up to the $1/f$ estimation in equation (10).

Finally, Fig. 20 is a plot of the infrared noise RMS as a function of UGF of the CARM feedback. This graph depicts the current noise requirement of 8 Hz, the current RMS, and the RMS assuming the acoustic noise is reduced by a factor of 10. This graph illustrates that the UGF of the CARM feedback can be increased up to 1 kHz while remaining under the noise requirement if the acoustic coupling can be reduced by a factor of 10 during the science run.

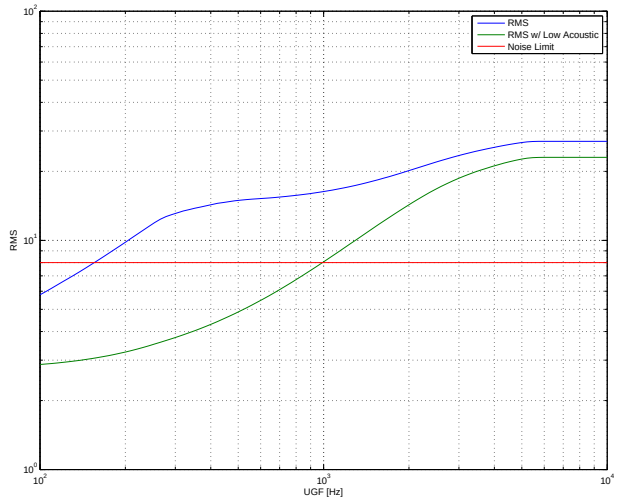

Figure 20: Infrared Residual RMS vs. UGF of CARM feedback

4 Conclusion

The ALS model generally replicates well the feedback servo controls implemented in HIFO-Y. The model provides the user with the ability to take transfer functions of individual or multi-stage loops. As outlined in Section 2 these transfer functions are reasonably close to that of the data (up to some gain factors and a few other discrepancies). In addition, the model has produced an overall noise budget depicting the main noise contributors. We have seen that the overall RMS falls below the noise requirement of 8 Hz. And more importantly, the model has indicated that with an improved acoustic noise, we can increase the UGF of the CARM feedback loop while still remaining under the predesignated noise requirement.

A Scripts

The model can be found under the file name:
/ligo/svncommon/40mSVN/aLIGO/HIFO/H1/.
The model is also accessible from svn from 40mSVN. This file is subdivided into utilities, data, and simulink files.

Table 2: MatLab Files and Description

Matlab File	**Description**
ALS_TFtestAO.m	Script that calls ALScontrolAO and creates the transfer functions.
Noisebudget.m	Script that call ALScontrolAO and imports data to create noise plots.
Noisebudgetmodern.m	Script that call ALScontrolAO and imports data to create noise plots. This script is different from the previous in that it includes the NB utility.
RMSvsUGF.m	Script that produces a plot of the RMS vs UGF of the CARM loop
/simulink/ALSControlAO.m	Script that calls the model and assigns parameter values.
/simulink/ALS_AO.mdl	ALS simulink model.
/data/	Contains all the measured transfer functions and power spectrums.
/util/makeZPK	Returns a ZPK object with field z, p, k, and sys (in Hz).
/util/makeZPKQ	Returns a ZPK object with field z, p, k, and sys (in Hz). with imaginary zeroes and/or poles.
/util/ConvertTF	Imports .ascii file and scans for data of the transfer function.
/util/ConvertTFv2	Merges two .ascii files; one with magnitude and the other with phase of a transfer function.
/util/ConvertTFv3	Merges two .txt files; one with magnitude and the other with phase (in deg) of a transfer function.
/util/FilterFunction	Reads a filter file.

Table 3 lists the poles and zeros (both in Hz) and the gain (specified in dB or magnitude) of each element in the control model as of July 30th, 2013. The transfer function of each loop is then given by

$$\mathrm{X}(f) = k\frac{\Pi_n(1+if/z_n)}{\Pi_m(1+if/p_m)} \tag{11}$$

where p_m are the poles, z_n are the zeroes, and k is the gain [6]. Meanwhile, Table 4 lists the filters used. Both tables are organized following the color scheme in Fig. 1:

Table 3: ALS Model Configuration

Element	Zeroes (Hz)	Poles (Hz)	Gain
F_EY_FIBR_SERVO	4k	1.35	-40dB [1]
A_EY_FIBR_SERVO	1e6, 0, 0 ± i*5125.05	100k, 0.85, -27.305 ± i*4124.97	0
A_EY_PZT	1e6	1e5	0
D_EY_FIBR_SERVO	–	1e-3	10
C_EY_REFL_SERVO	–	-600	600
H_EY_REFL_SERVO	0	-600	1
F_EY_REFL_SERVO	200, 1k	40, 100	-4dB or -8dB [2]
D_EY_REFL_SERVO	–	–	1.6281e-4 or 0
A_EY_REFL_SERVO	40	1.6	20k
D_PFD	–	1e-3	50
A_VCO	40	1.4	285,220
F_SR560	–	–	50
F_SR560v2	–	100	1
F_REFL_SERVO	–	–	0 dB
F_REFL_SERVO_FAST	.001, .001, 70k	5, 5, 140k	-32 dB
LSCCARMGain	–	–	10 * 8.46[4]
GainFast	–	–	0
GainSlow	–	–	0 or 1 [3]
GainMC	–	–	0dB
GainAO	–	–	2dB
C_IMC_REFL_SERVO	–	8812.36	1
H_IMC_REFL_SERVO	0	-8812.36	0
D_IMC_REFL_SERVO	–	–	2.2695e-5
F_IMC_REFL_SERVO	17k, 20k, 20k	40, 1k, 1k	0dB
F_IMC_REFL_SERVO_FAST	70k	140k	0dB
A_IMC_REFL_SERVO	40	1.6	268,302
IMCTEST	–	–	0 or 1
DC_CAL_M2	–	–	-11
DC_CAL_M3	–	–	-13
D_REF	–	–	-22dB
F_MC2_M3Gain	–	–	-1k
F_MC2_M2Gain	–	–	0.03

Table 4: Filters for ALS Model

Filters	TXT	Name	Modules On
F_REFL_SERVO_CARM	H1LSC.txt	LSC_CARM	FM1, FM3, FM4, FM5, FM6, FM6
F_REFL_SERVO_SLOW	H1LSC.txt	LSC_REFL_SERVO_SLOW	FM4, FM5, FM6
F_MC2_M2	H1SUSMC2.txt [5]	MC2_M2_LOCK_L	FM1, FM2, FM3, FM4, FM5, FM10
F_MC2_M3	H1SUSMC2.txt	MC2_M2_LOCK_L	FM4, FM5, FM6
A_MCL_M3	H1SUSMC2.txt	IMC_X_M2	FM6
A_MCL_M2	H1SUSMC2.txt	IMC_X_M3	FM6

B Images of End Y MEDM screens

As of July 23, 2013:

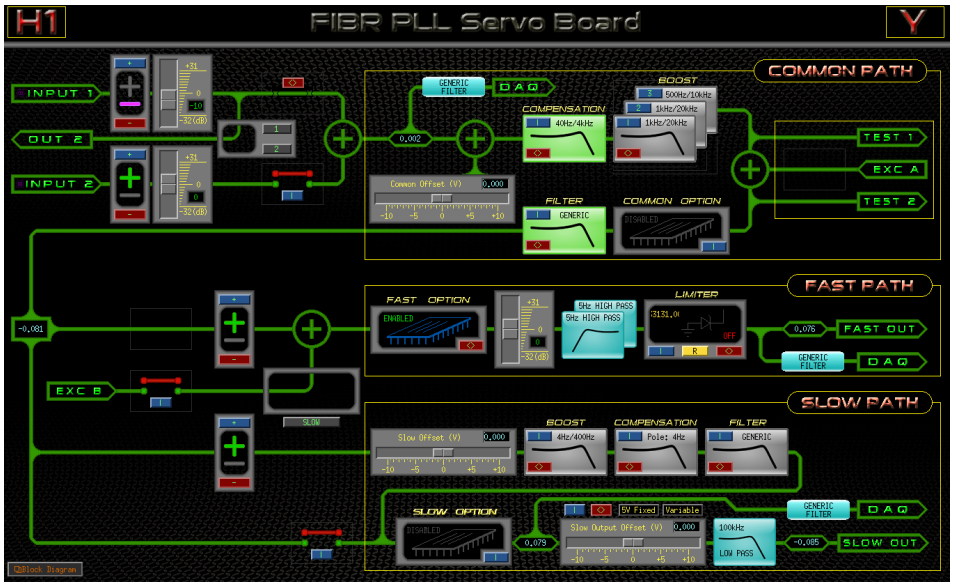

Figure 21: End Y FIBR Servo Board

[1] -10 dB comes from input 1 gain, while -30 dB comes from the board itself.
[2] Board is currently set to -8 dB; however data collected prior to July 25, 2013 was with -4 dB
[3] 1 or 0 is dependent on the transfer function being run; refer to matlab file for details.
[4] Mystery gain of 8.46.
[5] As of July 02, 2013

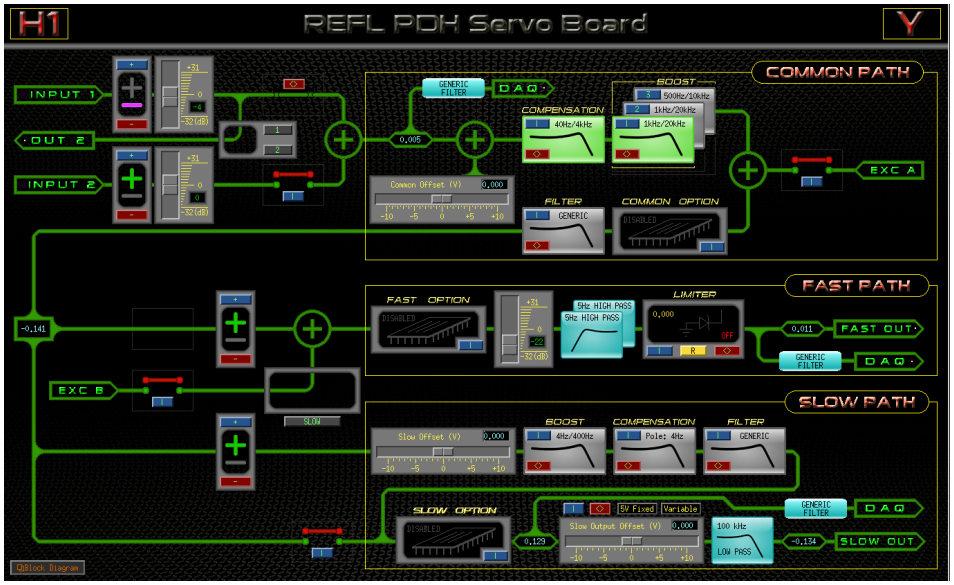

Figure 22: End Y REFL Servo Board

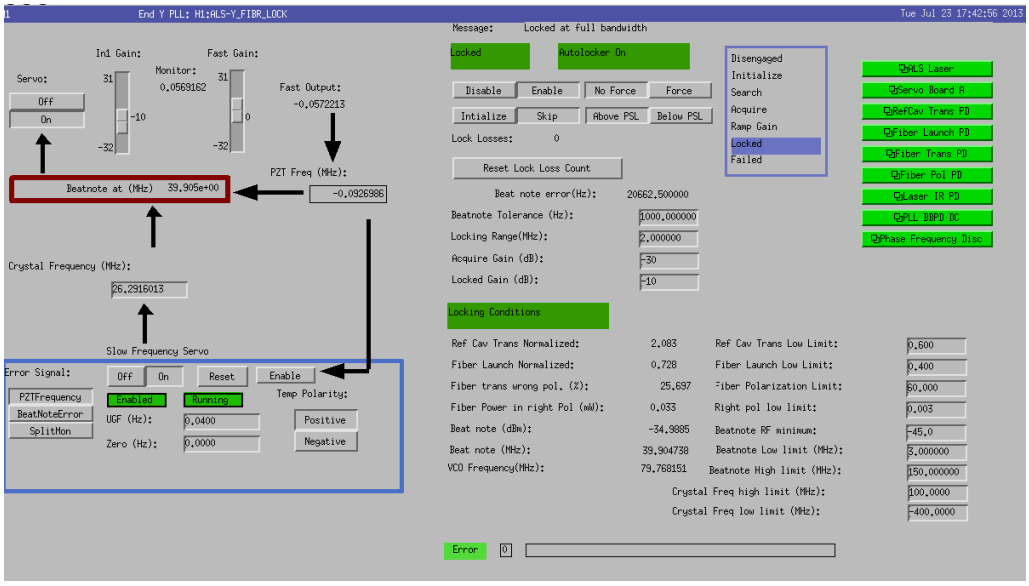

Figure 23: End Y FIBR Servo Autolocker

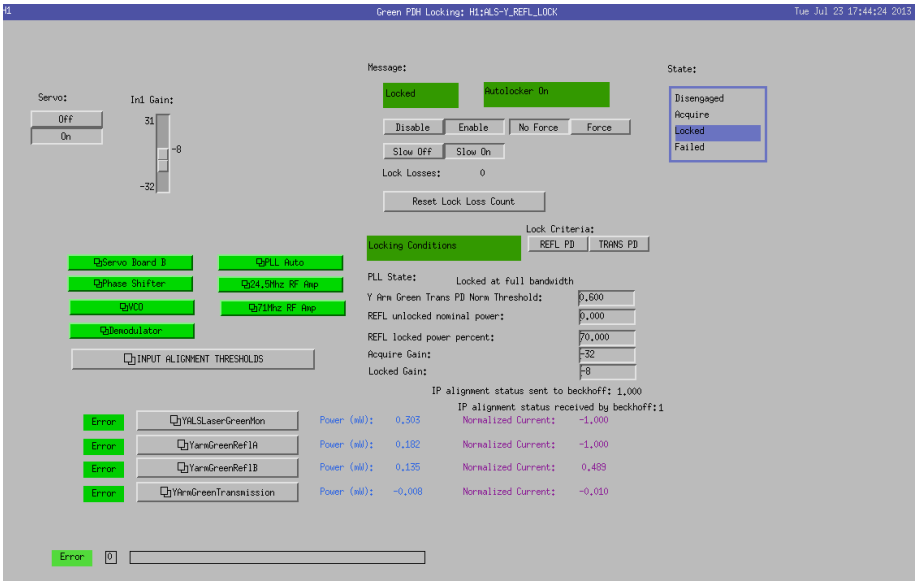

Figure 24: End Y REFL Servo Autolocker

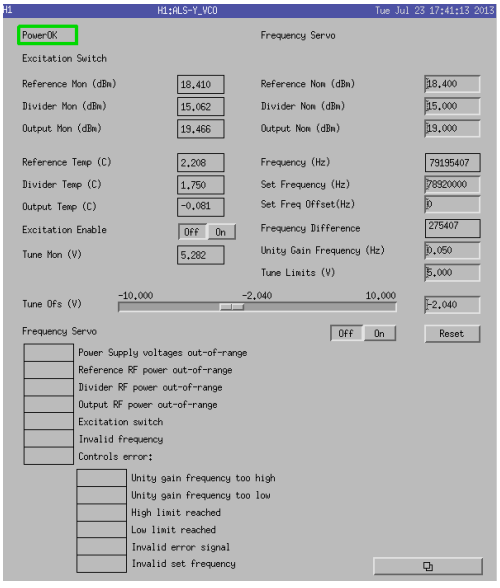

Figure 25: End Y VCO

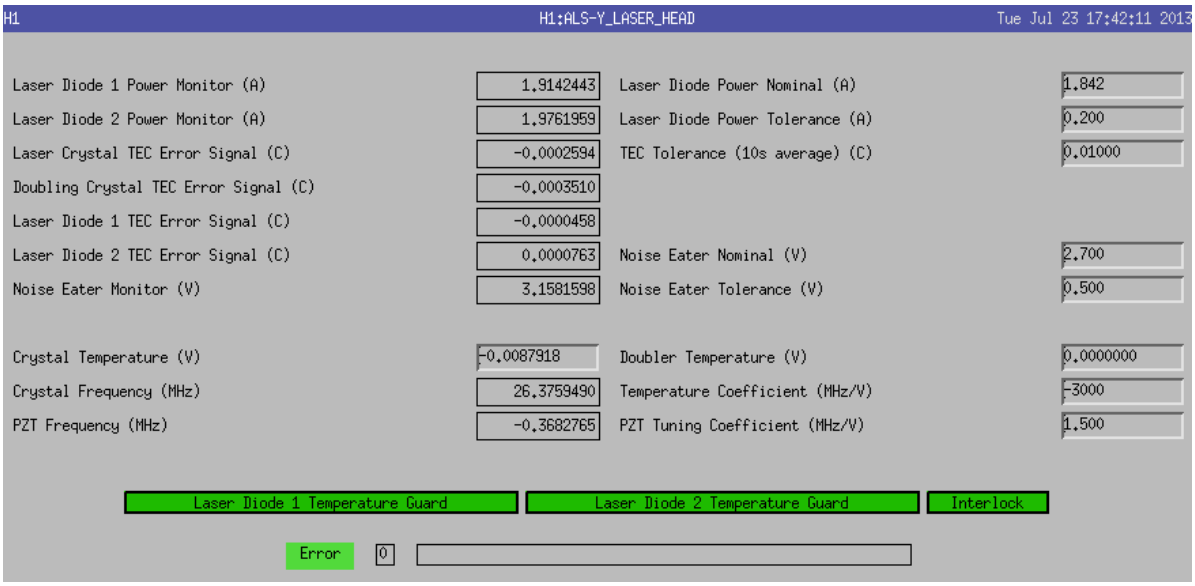

Figure 26: End Y Auxiliary Laser

References

[1] Matt Evans and et. al. Advanced ligo arm length stabilisation system design. LIGO-T0900144-v4-D, October 2010.

[2] L. Barsotti and M. Evans. Lock acquisition study for advanced ligo. LIGO-T1000294-v1.

[3] D. Sigg, K. Kawabe, and P. Fritschel. Commissioning advanced ligo's hifo-y. LIGO-T1300174-v1, March 2013.

[4] Bram Slagmolen and Daniel Sigg. Arm length stabilisation - fibre phase-locked-loop. LIGO-T1200429-v1, September 2012.

[5] Eric D. Black. An introduction to pound drever hall laser frequnecy stabilization. LIGO-P990042-A.

[6] Kiwamu Izumi. *Mutli-Color Interferometry for Lock Acquisition of Laser Interfeometric Gravitation-wave Detectors*. PhD thesis, The University of Tokyo, JULY 2012.

[7] Daniel Sigg. Phase frequency discriminator specification. LIGO-E1000450-v1.

[8] Jeffery Kissel. Summary of aligo sus model transfer functions. LIGO-T1200404-v1, August 2012.

[9] Lsc rfpd enclosure - in air - top assembly drawing. LIGO-D1101174-v5.

[10] Dick Gustafson, Ewan Douglas, Peter Fritschel, and Sam Waldman. Fiber phase noise measurements at lho. LIGO-T0900376-v1.

[11] Isaac Angert. Characterization of a voltage controlled oscillator. LIGO-T0900451-v1.

[12] D. Yeaton-Massey and R. X. Adhikari. A new bound on excess frequency noise in second harmonic generation in ppktp at the 10^{-19} level. *Opt. Express*, 2012.